



1 **Characterizing the evolution of mass flow properties and dynamics through analysis of**
2 **seismic signals: Insights from the 18 March 2007 Mt. Ruapehu lake-breakout lahar**

3

4 Braden Walsh¹, Charline Lormand², Jon Procter³, Glyn Williams-Jones¹

5 ¹Department of Earth Sciences, Simon Fraser University, Burnaby, British Columbia, Canada

6 ²Department of Earth Sciences, University of Durham, Durham, DH1 3LE, UK

7 ³Volcanic Risk Solutions, Institute of Agriculture and Environment, Massey University,

8 Palmerston North, New Zealand

9

10 Corresponding Author: Braden Walsh (braden_walsh@sfu.ca)

11

12 **Abstract**

13 Monitoring for lahars on volcanoes can be challenging due to the ever-changing landscape
14 which can drastically transform the properties and dynamics of the flow. These changes to the
15 flows require the need for detection strategies and risk assessment that are tailored not only
16 between different volcanoes, but at different distances along flow paths as well. Being able to
17 understand how a flow event may transform in time and space along the channel is of utmost
18 importance for hazard management. While visual observations and simple measuring devices in
19 the past have shown how lahars transform along the flow path, these same features for the



20 most part have not been described using seismological methods. On 18 March 2007 Mt.
21 Ruapehu produced the biggest lahar in New Zealand in over 100 years. At 23:18 UTC the tephra
22 dam holding the Crater Lake water back collapsed causing 1.3×10^6 m³ of water to flow out and
23 rush down the Whangaehu channel. We describe here the seismic signature of a lake-breakout
24 lahar over the course of 85 km along the Whangaehu river system using three 3-component
25 broadband seismometers installed <10 m from the channel at 7.4, 28, and 83 km from the
26 crater lake source. Examination of 3-component seismic amplitudes, peak frequency content,
27 and directionality combined with video imagery and sediment concentration data were used.
28 The seismic data shows the evolution of the lahar as it transformed from a highly turbulent out-
29 burst flood (high peak frequency throughout), to a fully bulked up multi-phase
30 hyperconcentrated flow (varying frequency patterns depending on the lahar phase) to a slurry
31 flow (bedload dominant). Estimated directionality ratios show the elongation of the lahar with
32 distance down channel, where each recording station shows a similar pattern, but for differing
33 lengths of time. Furthermore, using directionality ratios shows extraordinary promise for lahar
34 monitoring and detection systems where streamflow is present in the channel.

35 **1. Introduction**

36 Volcanic mass flows (e.g. debris flows, pyroclastic density currents, debris avalanches) are one
37 of the greatest threats to communities, industry, recreation, etc. on and around volcanoes.
38 These volcanic mass flows are particularly dangerous as they are fast moving turbulent flows
39 that can occur without any warning or an eruption transpiring (Capra et al., 2010). These flows
40 can move a sizable amount of liquid and debris great distances that can critically impact



41 locations hundreds of kilometers from the volcano or source. Lake-breakout or outburst flood
42 events can be particularly destructive because they tend to be larger and can cause long lasting
43 changes to the landscape and surrounding ecosystems (O'Connor et al., 2013; Procter et al.,
44 2021). Furthermore, unlike eruption or rain triggered mass flows, outburst floods have very
45 little to no warning. Eruption sources can be prepared for by the onset of the eruption and/or
46 the monitoring of the volcano through various methods (e.g. seismology, infrasound, gravity,
47 gas and water chemistry). Likewise, for rain-induced flows using techniques such as the amount
48 or intensity of rain (e.g. Capra et al., 2010; 2018) or by monitoring the amount of available
49 material (e.g. Iguchi, 2019) can help forecast when an event may occur.

50 In New Zealand, there have been numerous cases of large damaging mass flows in modern
51 times. In October 2012, a lake-breakout lahar originating from Te Maari, destroyed hiking trails
52 and forestry, eventually flowing over 4.5 km to damage and block off Highway 46 (Procter et al.,
53 2014; Walsh et al., 2016). Moreover, on 24 December 1953, the deadliest lahar in New Zealand
54 history occurred killing 151 people when a lahar struck a train crossing at the Tangiwai Rail
55 Bridge, 39.8 km from the Crater Lake on top of Mt. Ruapehu (O'Shea, 1954). The ability to
56 predict and investigate the changing dynamics and properties of large volcanic mass flows as
57 they progress down channel is the first step in beginning to understand flow mechanisms
58 better, and ultimately address the hazards involved to mitigate the risk.

59 In order to better characterize and understand these flow events, many applications and
60 instruments have been used in the past (e.g. trip wires, stage gauge, load cells, pore pressure).
61 While many of these tools can yield quick assessments and provide ample warning (e.g. current



62 meters, trip wires), they can sometimes be at risk of false detections, equipment damage or
63 loss, and/or lack the capability to evaluate the properties and dynamics of flow events.
64 Geophysical instruments (e.g. seismometers, geophones, infrasound) on the other hand can be
65 installed at a safe distance away from the channel and have shown signs of not only being
66 capable warning systems (e.g. Coviello et al., 2019), but have the ability to accurately estimate
67 flow properties (e.g. Arattano and Marchi, 2005; Doyle et al., 2010; Schimmel et al., 2021), as
68 well as flow dynamics (e.g. Gimbert et al., 2014; Coviello et al., 2018; Walsh et al., 2020). To this
69 extent, using geophysical instruments for mass flow monitoring is still relatively young and in
70 need of more comprehension, assessment and universality. One technique to increase the
71 ability to predict, warn, and estimate the properties and dynamics of flow events is to use all
72 three components of the seismic recording. Recently, several studies have shown that using all
73 three components is effective in characterizing flow events (e.g. snow-slurry lahars, Cole et al.,
74 2009; snow avalanches, Kogelnig et al., 2011; streamflow, Roth et al., 2016; landslides, Surinach
75 et al., 2005; lahars, Walsh et al., 2020; rockfalls, Kuehnert et al., 2021; hyperconcentrated
76 flows, Walsh et al., 2016). Using the horizontal components along with the vertical component
77 can yield additional information about the flow that was previously not recorded. Notably,
78 directionality analysis (e.g. Doyle et al., 2010; Walsh et al., 2020) can provide information about
79 wetted perimeter, sediment concentration, and number of particle collisions. Furthermore,
80 differing energies and frequency outputs from channel parallel and channel perpendicular
81 signals can point to specific changes within the flow (Burtin et al., 2010; Roth et al., 2016) that
82 can provide insights into the internal dynamics.

83 **1.1 Anatomy of lahars**



84 When a lahar is created from a lake-breakout or outburst flood event, the transition from flood
85 or streamflow torrent depends on the erosivity of the channel and the supply of sediment being
86 entrapped within the flow (e.g. Scott, 1988; Doyle et al., 2011). An event may start as a highly
87 turbulent low sediment flow, then transform into a hyperconcentrated flow, and may even
88 eventually 'bulk up' to exhibit characteristics of a debris flow with the possibility of laminar or
89 plug-like behavior (Scott, 1988, Pierson et al., 1990). At Mt. Ruapehu, the propagational
90 differences of lahars down channel have been observed and characterized in the past (e.g.
91 Cronin et al., 1996; Cronin et al., 1999; Cronin et al., 2000; Manville et al., 2000; Procter et al.,
92 2010a; Lube et al., 2012). From these studies, models of how lahars bulk up and transition
93 throughout the run-out distance have been postulated. For the lahars in the Whangaehu
94 channel, Cronin et al. (1999) created three 4-phase conceptual models based on source
95 distances of 23.5 km, 42 km, and >55 km. The first two models are for lahar regimes, whereas
96 the third model described a lahar almost at its peak run-out distance. In each model, the first
97 phase consists of a super charged streamflow pulse that flows ahead of the head of the flow.
98 This phenomenon has also been noted for debris flows interacting with streamflow (Arattano
99 and Moia, 1999). Furthermore, discharge is maximum at the transition between phase 1 and
100 phase 2 (Cronin et al., 1999). Phase 2 is described as a mixing zone between streamflow and
101 increasing sediment content, where the peak sediment concentration usually occurs at the end
102 of phase 2 or at the beginning of phase 3 (e.g. Pierson and Scott, 1985). Cronin et al. (1999)
103 defined phase 3 as the lahar body, which has the least amount of the original streamflow
104 contained within. Phase 3 is also characterized by coarse sediment suspensions and is the most
105 likely location for debris flow rheology. Finally, phase 4 is the tail of the lahar where debulking

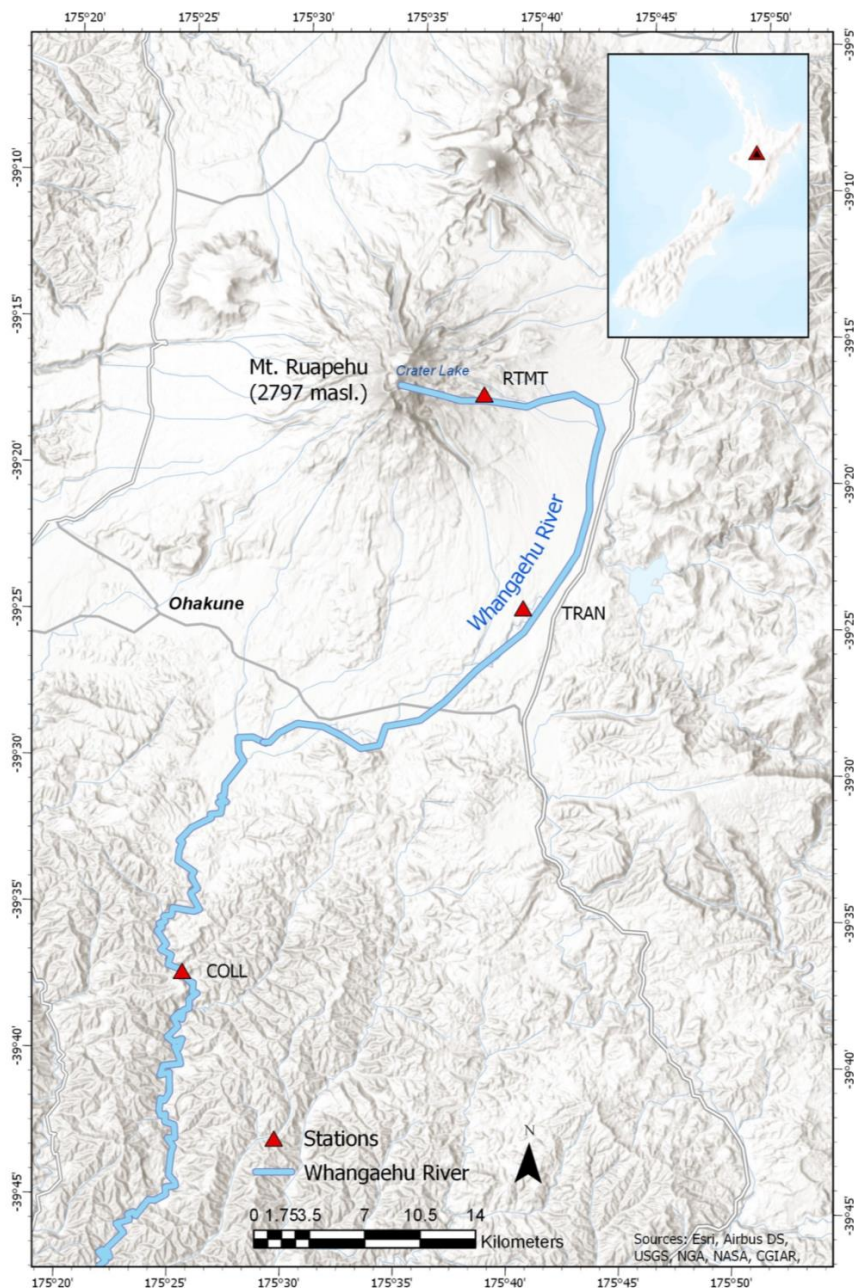


106 and dilution occurs transforming the lahar back into a hyperconcentrated, mixed, or
107 streamflow.

108 **1.2 18 March 2007 lake-breakout event**

109 Mt. Ruapehu (2797 asl) is the largest stratovolcano in the central North Island of New Zealand
110 (Figure 1) which sits at the southwestern end of the Taupō Volcanic Zone (TVZ). The volcano has
111 a volume of 110 km^3 which is composed of several overlapping cone building formations and
112 surrounding ring plain volcanoclastics (Carrivick et al., 2009; Pardo et al., 2012). On top of the
113 volcano, above the currently active vent sits a $1 \times 10^7 \text{ m}^3$ acidic crater lake (Procter et al., 2010a).
114 The Whangaehu River is the preferred outlet for Crater Lake water and lahars in recent history
115 (Procter et al., 2012; Procter et al., 2021). The Whangaehu River channel is on the eastern flank
116 of Mt. Ruapehu where it runs down across the volcanic ring plane where it eventually heads
117 southwest for $\sim 200 \text{ km}$ reaching the Tasman Sea.

118 Prior to the events that took place in the morning local time on 18 March 2007, a heavy
119 rainstorm occurred accumulating about 256 mm of water over the 10 hours prior to the dam
120 breach that led to the outburst flood (Massey et al., 2010). The intense rain caused the Crater
121 Lake to rise an extra 6.4 m above the natural lava formation ledge, which started to cause
122 seepage and extra water entering the Whangaehu gorge (Carrivick et al., 2009). At $\sim 11:18 \text{ NZT}$
123 (GMT +12), the tephra dam collapsed causing $1.3 \times 10^6 \text{ m}^3$ of water to flow out of the lake and
124 into the Whangaehu channel (Procter et al., 2010a). The dam was eroded and undercut in
125 multiple stages resulting in a series of retrogressing landslides along with the main debris
126 flow/lahar channel.



127

128 *Figure 1 Map of Mt. Ruapehu and the surrounding area located on the central North Island of New Zealand. Blue*
129 *outline represents the Whangaehu channel and the path the 18 March 2007 lahar traveled down. Red triangles*
130 *denotes the three monitoring stations along the Whangaehu channel at 7.4, 28, and 83 km.*



131 Since the lahar was caused by lake-breakout dynamics and thus an abundance of water, the
132 event was classified as a hyperconcentrated streamflow rather than a sediment-filled debris
133 flow (Procter et al., 2010b). At ~8.0 km from source velocity measurements recorded the flow
134 at ~ 9.5 m/s and had an estimated 6 m of downcutting showing the ability for the lahar to
135 deposit and erode massive amounts of material (Procter et al., 2010a,b). Furthermore, the 18
136 March 2007 lahar was one of the most thoroughly monitored lahars ever (Manville and Cronin
137 2007). In total there were 21 monitoring locations setup to measure various lahar properties
138 (e.g. flow monitor, camera, stage height, flow sampling, pore-pressure, seismic, etc.) along the
139 channel (Keys and Green, 2008; Lube et al., 2012), with the lahar taking over 16 hours to
140 eventually travel out to the New Zealand coast, ~200 km from the original crater lake source.

141 Here, we delve into the properties of a lake-breakout hyperconcentrated streamflow that
142 bulked up to a volume of $\sim 4.4 \times 10^6 \text{ m}^3$ (Procter et al., 2010a) over the course of 83 km that
143 occurred on 18 March 2007 along the Whangaehu River channel originating from Mt. Ruapehu,
144 New Zealand. The combination of seismic analysis (frequency and directionality) with on-the-
145 ground measurements (e.g. video, sediment concentration) show how a lahar transforms over
146 time and distance and how using these seismic techniques can help monitor the ever changing
147 dynamics and properties of a flow event. Furthermore, we examine previous models of the
148 evolution of a lahar and compare the model with the seismic data available.

149 **2. Data**

150 The seismic data for the 18 March lahar was recorded on three seismometers installed at
151 various distances (7.4, 28, 83 km) along the Whangaehu channel (Figure 1). The three 3-



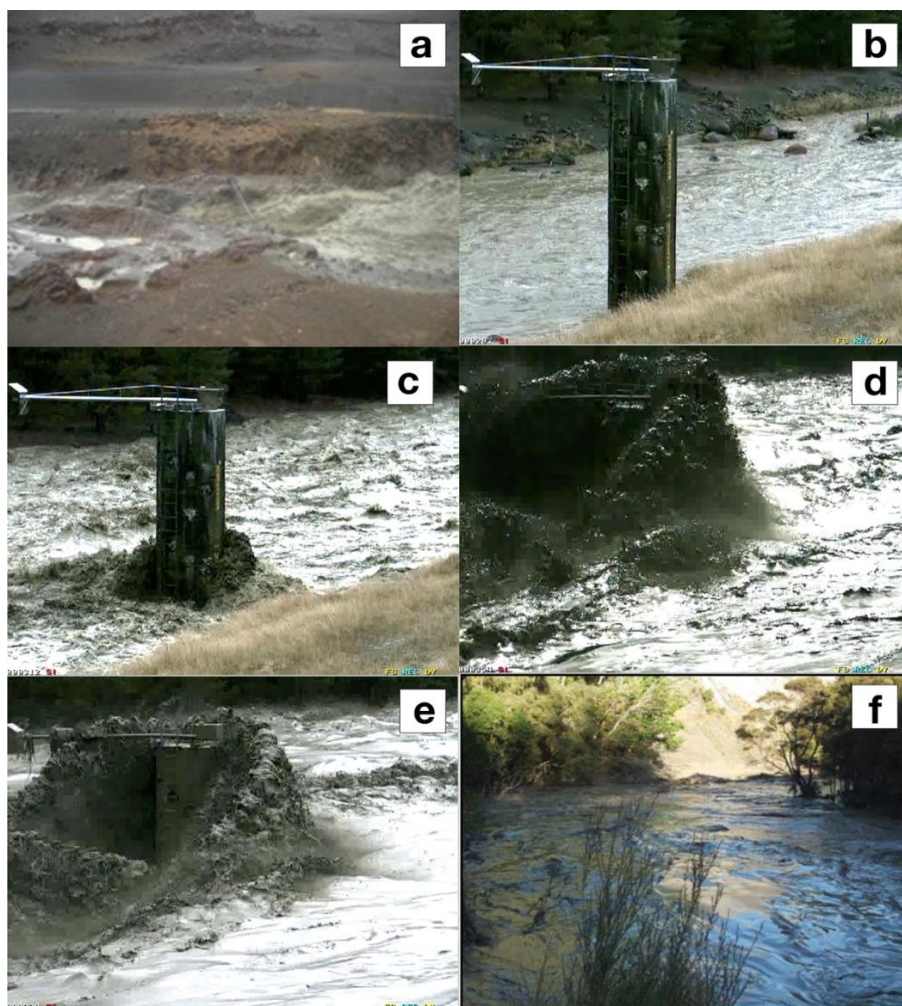
152 component broadband Guralp 6T sensors (COLL, RTMT, TRAN) recorded data at 100 Hz
153 sampling and had GPS time stamps. For each site, the seismometers axes were installed to true
154 North and the recorded data were rotated to align North as flow parallel (P) and East as the
155 cross-channel direction (T). The monitoring station Round the Mountain Track (RTMT), was
156 installed 4 m from the channel and 7.4 km downstream from the source of the lahar. The lahar
157 arrived at RTMT at 11:36 UTC and had an average velocity of 9.3 m/s (Figure 2a). The Trans Rail
158 Gauge (TRAN) station was installed 28 km from source and 10 m from the channel, which also
159 included a video camera that captured an image every 30 seconds. The lahar arrived at TRAN at
160 12:35 UTC with an average velocity of 5.6 m/s (Figure 2d). The Colliers Bridge (COLL) station
161 was installed 10 m from the channel and 83 km from source. The lahar arrived at COLL at 16:13
162 UTC and had an average velocity of 4.8 m/s (Figure 2f).

163 **3. Results**

164 To examine the multi-component dynamics of the 18 March lake-breakout event along the
165 Whangaehu channel at three monitoring locations, the data were corrected for instrument
166 response and split into 10 s time windows. At each recording location, peak spectral frequency
167 (PSF) amplitude, root mean squared (RMS) amplitude, and directionality ratios (DR) are
168 estimated. At each monitoring station the first hour of the lahar including five minutes prior to
169 the arrival are shown in all the results except when indicated.

170

171



172

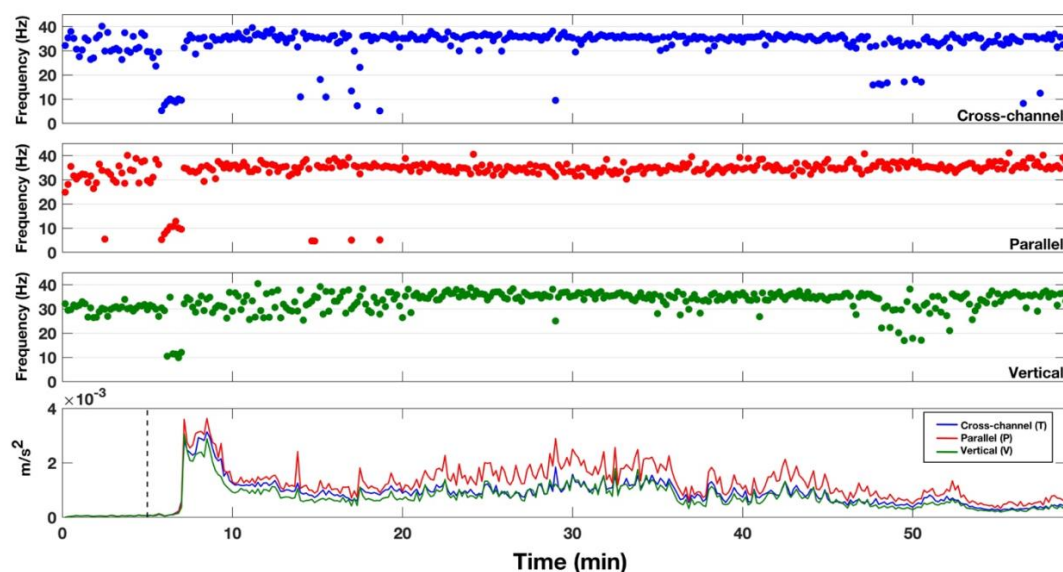
173 *Figure 2 Images from the 18 March 2007 lake break-out lahar from RTMT (a), TRAN (b, c, d, e), and COLL (f). Note*
174 *the transformation of the lahar at TRAN from streamflow (b), increased discharge pre-lahar phase 1 pulse (bow*
175 *wave) (c), head of the lahar (d), and low PSF beginning of lahar body (e).*

176 3.1 Frequency analysis

177 In order to examine the PSFs for all three components at each site along the channel, we use
178 the frequency recorded at the maximum amplitude of the frequency spectra for each 10 s
179 running time window. The PSF for RTMT (7.4 km from source) shows similar patterns between



180 all three components (Figure 3). Five minutes prior to the arrival of the head (peak seismic
181 amplitude) of the lahar (streamflow) are characterized by scattered PSFs between 20-40 Hz for
182 the cross-channel (Figure 3, blue dots) and parallel (Figure 2, red dots) directions, while in the
183 vertical direction (Figure 3, green dots) the PSF is ~ 30 Hz. When the front of the lahar arrives at
184 the station the PSF in all three components decreases to ~ 5 -10 Hz for about 1 min before
185 increasing again to higher frequencies. After front of the lahar passes the station and when the
186 head arrives (peak seismic amplitude) the PSF in the cross-channel and parallel directions
187 remain between 30-40 Hz for the rest of the recording window. In the vertical component, the
188 PSF is scattered between 20-40 Hz for ~ 15 min after the arrival of the head of the lahar and
189 then becomes narrower, similar to both the cross-channel and parallel components with PSFs
190 between 30-40 Hz.



191

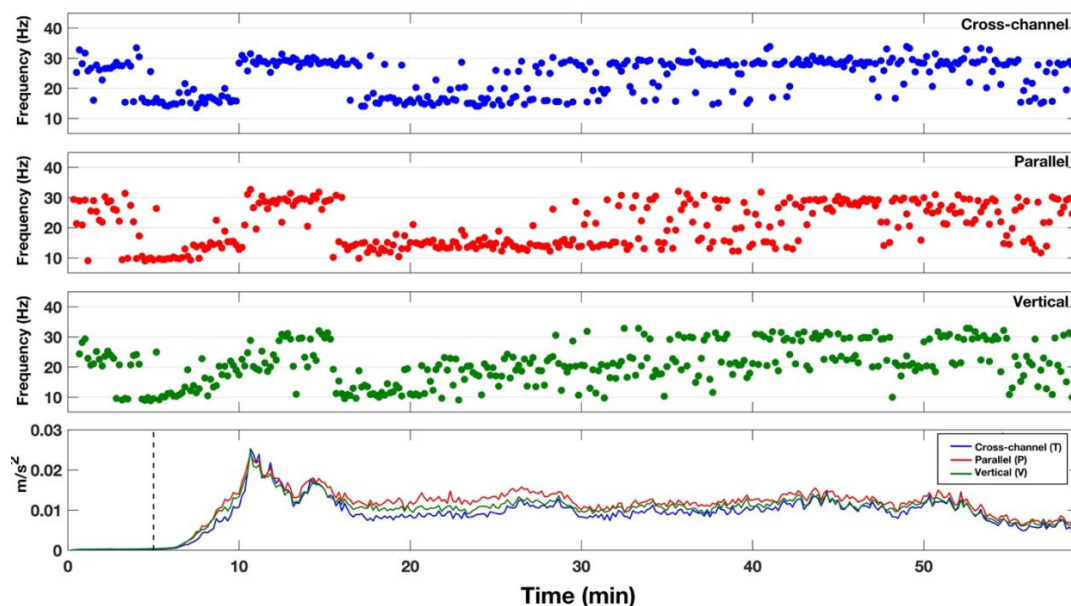
192 *Figure 3 Peak spectral frequencies for RTMT (7.4 km from source) for cross-channel (blue dots), flow parallel (red*
193 *dots), and vertical (green dots) directions. Bottom row depicts the RMS amplitude of the lahar passing the station*



194 *color coded to the same colors as the PSF. The dashed vertical line marks the timing of the lahar front passing the*
195 *monitoring station. All PSFs and RMS amplitudes were calculated using 10 s time windows.*

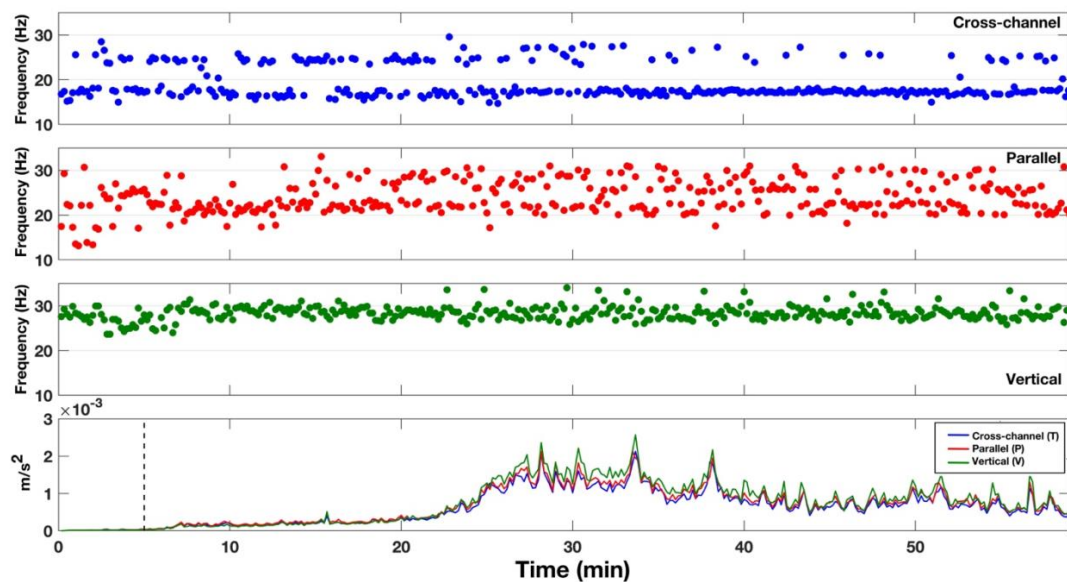
196 Further down the channel at station TRAN (28 km from source), the PSFs for all three
197 components show a similar overall pattern (Figure 4). The pre-lahar PSF distribution in all three
198 components is between 20-32 Hz. Like RTMT higher up the channel, the PSFs for the front of
199 the lahar at TRAN first drops down to around 10 Hz and when the lahar head arrives (10 min,
200 Figure 4) the PSF increases to ~30 Hz for parallel (Figure 4, red dots) and cross-channel (Figure
201 4, blue dots) directions and between 20-30 Hz in the vertical component. This decrease to
202 lower frequencies before the head of the lahar at TRAN lasts for about 5 min. After the head of
203 the lahar passes the recording station the PSF content decreases for ~15 min to 10-20 Hz for
204 the parallel and cross-channel components and between 10-25 Hz for the vertical (Figure 4,
205 green dots) components. The PSF after the 30 minute mark in Figure 4 displays a bimodal
206 pattern with frequencies between 10-35 Hz, with PSF time windows concentrating most at ~30
207 Hz.

208 At the COLL recording station (83 km from source), the PSF distribution shows differing patterns
209 for all three components (Figure 5). The PSF in the cross-channel direction (Figure 5, blue dots)
210 depicts a bimodal pattern throughout with a strong lower concentration of time windows at
211 ~18 Hz and a higher PSF at ~25 Hz. For the parallel component (Figure 5, red dots), the pre-
212 lahar signal has a wide PSF range between 12-30 Hz. When the lahar arrives, the PSF becomes
213 concentrated at ~22 Hz for ~8 min before transforming into a bimodal pattern similar to that of
214 the cross-channel PSF, with frequencies between 20-30 Hz. In the vertical component (Figure 5,
215 green dots), the PSF remains concentrated around ~28 Hz, only varying just prior to the arrival
216 of the lahar and during the highest energy stage of the lahar (25-40 min).



217

218 *Figure 4 Peak spectral frequencies for TRAN (28 km from source) for cross-channel (blue dots), flow parallel (red*
219 *dots), and vertical (green dots) directions. Bottom row depicts the RMS amplitude of the lahar passing the station*
220 *color coded to the same colors as the PSF. The dashed vertical line marks the timing of the lahar front passing the*
221 *monitoring station. All PSFs and RMS amplitudes were calculated using 10 s time windows.*



222

223 *Figure 5 Peak spectral frequencies for COLL (83 km from source) for cross-channel (blue dots), flow parallel (red*
224 *dots), and vertical (green dots) directions. Bottom row depicts the RMS amplitude of the lahar passing the station*
225 *color coded to the same colors as the PSF. The dashed vertical line marks the timing of the lahar front passing the*
226 *monitoring station. All PSFs and RMS amplitudes were calculated using 10 s time windows.*

227 3.2 Directionality

228 When recording mass flows with 3-component sensors, the directionality may be examined due
229 to the sensor being able to record signals in the two horizontal directions. The directionality
230 ratio allows for the determination of which horizontal component has the stronger energy over
231 the course of the recording window. This is possible because, in channel side deployments for
232 mass flow monitoring systems, the sensor is either installed aligned to North as flow parallel or
233 can be rotated during the data processing stage to align with the channel orientation.
234 Furthermore, with the channel side installations, attenuational factors can mostly be ignored
235 due to the close proximity to the channel and energy output of the flow event. The
236 directionality ratio (DR) can be defined as the cross-channel energy divided by the flow parallel



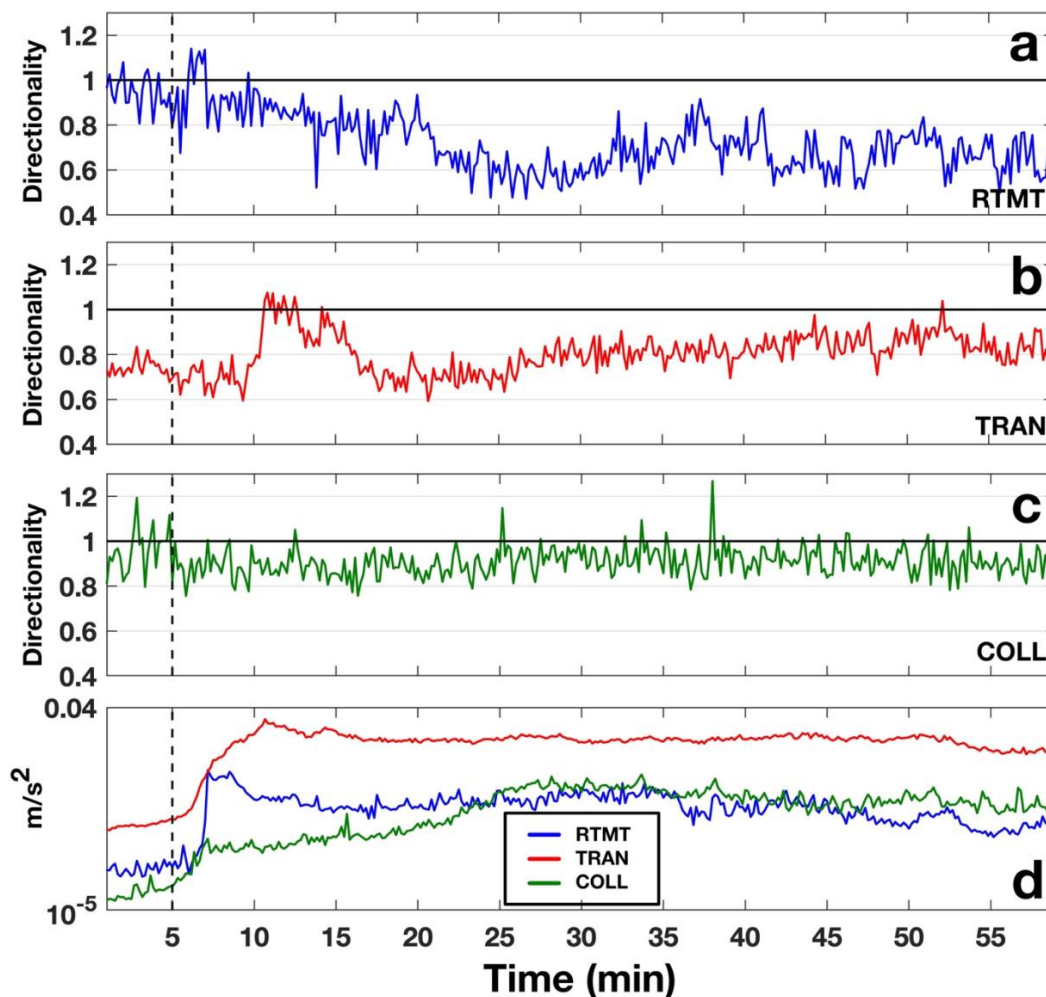
237 energy. A $DR > 1$ indicates that the cross-channel energy is larger than that of the flow parallel,
238 and vice-versa for a $DR < 1$. Directionality ratios have been used in the past to show rheology
239 changes within flows for warning purposes (Walsh et al., 2020), and have been hypothesized to
240 be an indicator for flow properties such as sediment concentration, wetted perimeter, and/or
241 amount of particle collisions within a lahar (Doyle et al., 2010).

242 The directionality ratios for 10 s running time windows at each seismic station for the 18 March
243 2007 lake-breakout lahar are shown in Figure 6. The DR for RTMT (Figure 6a) displays a DR
244 around 1 pre-lahar, then decreases right before the lahar arrives at the recording station
245 (Figure 6, dashed line), then as soon as the lahar passes, the DR increases to above $DR = 1$ for
246 ~ 2 min. After the initial lahar flood pulse passes RTMT, the DR then proceeds to decrease below
247 a $DR = 1$ for the rest of the recording window. Similar to RTMT, the DR for TRAN starts out with
248 a $DR < 1$ (0.7-0.8) and as the lahar front passes, the DR similarly decreases to 0.6-0.7 before
249 increasing to a $DR > 1$ when the lahar is at peak energy output at the 10 min mark (Figure 6d,
250 red line). After the passing of the peak energy, the DR for TRAN decreases below 1 again for the
251 remainder of the recording window. Further down the channel at COLL (Figure 6c), the DR
252 before the lahar arrives has a wide range of values between 0.8-1.2. When the front of the
253 lahar passes (Figure 6, dashed line), the DR stabilizes between 0.8-1, before increasing slightly
254 when the peak energy of the lahar passes the monitoring site.

255

256

257



258

259 *Figure 6 Directionality ratio plots over time for RTMT (a), TRAN (b), and COLL (c). Vertical RMS seismic signals for*
260 *the three stations are plotted in (d) where blue is RTMT, red is TRAN and green represents COLL. The dashed*
261 *vertical lines mark the timing of the lahar front passing the monitoring station. All DRs and RMS amplitudes were*
262 *calculated using 10 s time windows.*

263 4. Discussion

264 4.1 Evolution of lahar signals



265 A lahar propagating down channel can bulk up by collecting material from erosion or through
266 the combination of multiple pulses (Procter et al., 2010; Doyle et al., 2011). Lahars can also
267 debulk by depositional means or by the natural elongation of the lahar as it progresses down
268 channel (Doyle et al., 2011; Lube et al., 2012). Considering the 18 March 2007 lake-breakout
269 lahar was a large pulse of water that only mixed with the existing streamflow and contained no
270 juvenile material, examining the seismic signatures along the flow path can be used to
271 characterize the evolution and transformation of a lake-breakout event from outburst flood to
272 hyperconcentrated flow and beyond. At RTMT (Figure 3), the seismic signature is dominated by
273 the flow parallel direction with > 30 Hz PSF. The exception to this is the timeframe immediately
274 before the head of the lahar passes when the PSF decreases to ~ 10 Hz. This low frequency
275 signal can be seen at TRAN (Figure 4) and in the flow parallel component at COLL (Figure 5, red
276 dots). However, at COLL the PSF is ~ 20 Hz instead of 10 Hz as in RTMT and TRAN due to flow
277 properties at 83 km from source. This low PSF before the head of the lahar arrives at the station
278 could represent the supercharged stream flow pulse (bow wave) that is pushed in front of the
279 head of the lahar as described by Cronin et al. (1999) where they noticed these same pulses in
280 front of lahar heads for three lahars on Mt. Ruapehu in 1995. Conversely, this frontal pulse
281 could be from the uplift of streamflow from the faster moving underflow of the lahar (Manville
282 et al., 2000). Furthermore, the low frequency zone before the head of the flow lengthens as the
283 lahar progresses downstream, suggesting that lahar elongation can also be seen in the seismic
284 frequency domain. The ~ 10 Hz PSF may be explained by flow processes (Schmandt et al., 2013;
285 Barriere et al., 2015; Bartholomaeus et al., 2015) and could be due to the flow at this stage being
286 more sensitive to discharge (Gimbert et al., 2014; Schmandt et al., 2017; Anthony, et al., 2018)



287 or in the case of the underflow hypothesis, frictional sliding on the channel bed (Huang et al.,
288 2004). The frontal surge or phase 1 of the lahar can be seen in the DR (Figure 6) as well. For
289 every station along the channel the DR has a slight drop when phase 1 passes the recording
290 station (Figure 6, dashed line). The elongation of phase 1 can also be seen, where the dip in the
291 DR is only ~1 min for RTMT, ~5 min for TRAN, and approximately 20 min for COLL. The reason
292 the DR decreases during phase 1 for the 2007 lahar could be due to the parallel component
293 being more sensitive to flow processes than bedload forces (Barriere et al., 2015; Roth et al.,
294 2016). During phase 1 discharge increases, sediment concentration is low, and streamflow
295 dominates resulting in a low DR. The low DR can also be seen before the arrival of phase 1, due
296 to streamflow already occurring in the channel. The higher flow parallel energy over cross-
297 channel energy for streamflow has also been noted in the past for lahars at Volcán de Colima,
298 Mexico (Walsh et al., 2020).

299 Following the low PSF phase 1 (i.e. front of the lahar), the peak seismic amplitude occurs. The
300 peak seismic amplitude for RTMT is accompanied by an increase to higher PSFs > 30 Hz (Figure
301 3). PSFs > 30 Hz have been shown in the past to be either dominated by turbulence or bedload
302 transport (e.g. Gimbert et al., 2014; Roth et al., 2016). The 2007 lake-breakout lahar has been
303 described as a hyperconcentrated streamflow (e.g. Procter et al., 2010b) with low sediment
304 concentration, especially early on before the lake water captured enough material to bulk up
305 into a full 4-phase lahar. At RTMT, which was only 7.4 km from source, the lahar had not fully
306 bulked up yet and was in a net depositional regime (Procter et al., 2010a). Due to the
307 conditions of the lahar at RTMT, we surmise the higher PSF content for the peak seismic
308 amplitude is dominated by turbulent-flow-induced noise. Furthermore, the higher PSF content



309 at RTMT compared to TRAN and COLL (~30 Hz) could be due to the angle of the slope at the
310 recording stations. Gimbert et al. (2014) noted that turbulence noise will dominate over
311 bedload-induced noise on steeper slopes. Further down the channel at TRAN, the PSF for the
312 peak seismic amplitude is ~30 Hz for all three components. Again, this high PSF can be
313 attributed to turbulence as seen by the images taken at TRAN (Figure 2d). The difference at
314 TRAN is the length of the higher PSF, where at RTMT the high PSF stays throughout the entirety
315 of the recording window, at TRAN the high PSF and seismic amplitude only last for ~5 min. The
316 difference at TRAN could be from the evolution of the lahar. By time the lahar reached the
317 monitoring station at TRAN (28 km from source) the lahar was fully bulked up and had the
318 properties of a traditional four phase lahar as described by Scott (1988) or Cronin et al. (1999).
319 By time the lahar reached COLL 82 km from source the peak seismic amplitude is associated
320 with PSFs between 15-30 Hz, with bimodal patterns in the horizontal components and a tighter
321 spread in the vertical component (~27-29 Hz). At COLL, the lahar had converted into a plug-like
322 flow with lower turbulence and hence the higher PSFs are most likely associated with bedload
323 transport (Figure 2f). Furthermore, Burtin et al. (2010) and Roth et al. (2016) noted that when
324 the vertical component has greater seismic amplitudes than the horizontal components,
325 bedload dominates. This same amplitude feature can be seen at COLL (Figure 5, bottom panel)
326 where the vertical energy is greater than each of the horizontal components. The bimodal
327 pattern of the horizontal components is likely to be the recording of both turbulence or flow
328 properties (lower PSF) and bedload transport (higher PSF). This also explains why the vertical
329 component does not show the same bimodal pattern. Barriere et al. (2015) described the
330 parallel component as being more sensitive to flow properties, and Doyle et al. (2010) noted

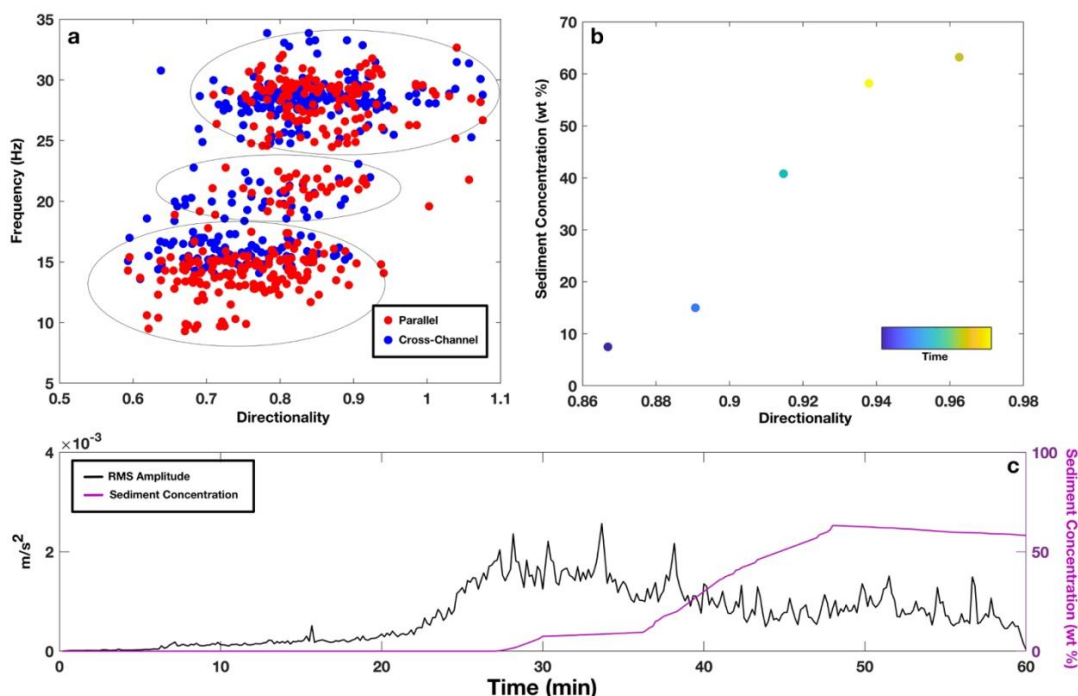


331 that the cross-channel component is likely dominated by turbulence, thus the reasoning behind
332 the differing PSF patterns between components. This PSF feature is similar to the lahars
333 recorded by Walsh et al. (2020), where the cross-channel PSF is confined within a narrow band
334 around 15-20 Hz and the flow parallel PSF is more bimodal. At COLL, the cross-channel PSF is
335 dominated by PSFs at ~18 Hz (lower than vertical component at ~28 Hz), with the flow parallel
336 between 20-30 Hz.

337 The DR at the peak seismic amplitude for all three recording stations increases (Figure 6). The
338 DR for both RTMT and TRAN increases to $DR > 1$. Doyle et al. (2010) noted that higher wetted
339 perimeters will increase the DR, which is true for the 18 March 2007 lake-breakout lahar (Figure
340 6, peak DR/RMS amplitude). Conversely, the DR decreases after the peak seismic amplitude
341 while the wetted perimeter is still high. Also, at COLL the DR only increases slightly with the
342 seismic amplitude. While the wetted perimeter may be a factor in increasing cross-channel
343 energy and thus the DR, the more likely explanation for the 18 March 2007 lahar might be the
344 higher level of particle collisions at the peak seismic amplitude. More particle collisions would
345 increase the DR (e.g. Doyle et al., 2010) due to more lateral excitation within the flow and
346 against the channel walls. The increase in collisional energy also relates well with the PSF, as
347 higher PSF correlates to an increase in the amount of interflow collisions as shown by Huang et
348 al. (2004) and may also explain why DRs correlate well with PSF (Figure 7a). The DR for COLL
349 during this same timeframe probably is not due to the amount of particle collisions due to the
350 plug-like flow (Figure 2f), but rather the increase in sediment concentration (Figure 7c). As the
351 sediment concentration increases at COLL the DR starts to increase as well (Figure 7b). Similar
352 to Doyle et al. (2010), COLL yields a correlation between DR and sediment concentration (Figure



353 7b), where higher DRs indicate higher concentrations of sediment contained in the flow. Lastly,
354 as noted above, DRs may correlate with PSF or at least indicate differing processes taking place
355 within the flow (Figure 7a). Lower PSF would produce lower DRs because low PSF are more
356 sensitive to flow processes (hence higher parallel energy) whereas higher PSFs would produce
357 higher DRs due to higher PSF being dominated by collisions and turbulence (higher cross-
358 channel energy) (Figure 7a).



359

360 Figure 7 Plots of (a) correlation between PSF and DR at TRAN, (b) sediment concentration and DR at COLL, and (c)
361 seismic amplitude (black line) with sediment concentration (purple line) depicting the lag in sediment at COLL. Note
362 that at COLL the first sediment concentration measurement did not occur until the 30 min mark.

364 While the lahar at RTMT was a large outburst flood/sediment-laden flow, and at COLL a plug-
365 like flow, at TRAN the 18 March 2007 lahar was a dynamic bulked up “traditional” lahar. The
366 evidence for this is in the PSF content for TRAN (Figure 4) compared to the other two



367 monitoring sites. At TRAN the PSF has a step-up step-down pattern for the first 30 min of the
368 lahar passing, and then transitions to a bimodal or wide PSF range for the rest of the recording
369 window. As noted above, the low PSF preceding the lahar head arrival is thought to be due to a
370 sensitivity to water transport properties (Figure 2c). The increase to higher PSFs during the peak
371 seismic amplitude may be from particle collisions and/or higher turbulence (Figure 2d). After
372 the maximum seismic amplitude at TRAN, the PSF decreases to 10-20 Hz. This drop in PSF after
373 the highest stage and amplitude could be from a more water transport dominated regime,
374 which can be seen in the increased parallel amplitude (Figure 4, 7a). The decrease may also be
375 from greater frictional sliding on the channel bed (Huang et al., 2004). Furthermore, this PSF
376 range could simply indicate a decrease in turbulence (Figure 2e). After the decrease to 10-20 Hz
377 PSFs, the PSF displays a bimodal or wide frequency range at ~28 min (Figure 4). As
378 aforementioned for COLL, this PSF pattern could be from both bedload- and water-transport-
379 induced noise. This timeframe is also where the peak sediment concentration would be, as
380 noted by Cronin et al. (1999), and thus the PSF would show more bedload high PSF. This
381 hypothesis also compares well with the DR (Figure 6b), where the cross-channel energy
382 increases starting at ~25 min indicating that the sediment concentration may be increasing
383 (Doyle et al., 2010). Finally, the wide PSF range later in the recording window (Figure 4) could
384 also result from the lahar having two distinct layers as described by Cronin et al. (2000), where
385 there is a wide more dilute finer grain top layer and a channelized sediment-rich layer on the
386 bottom. The two layer model can apply to TRAN because the lahar at this monitoring station
387 overtook the channel (Figure 2d,e) and proceeded to flow horizontally outward forming the
388 surface layer described by Cronin et al. (2000).

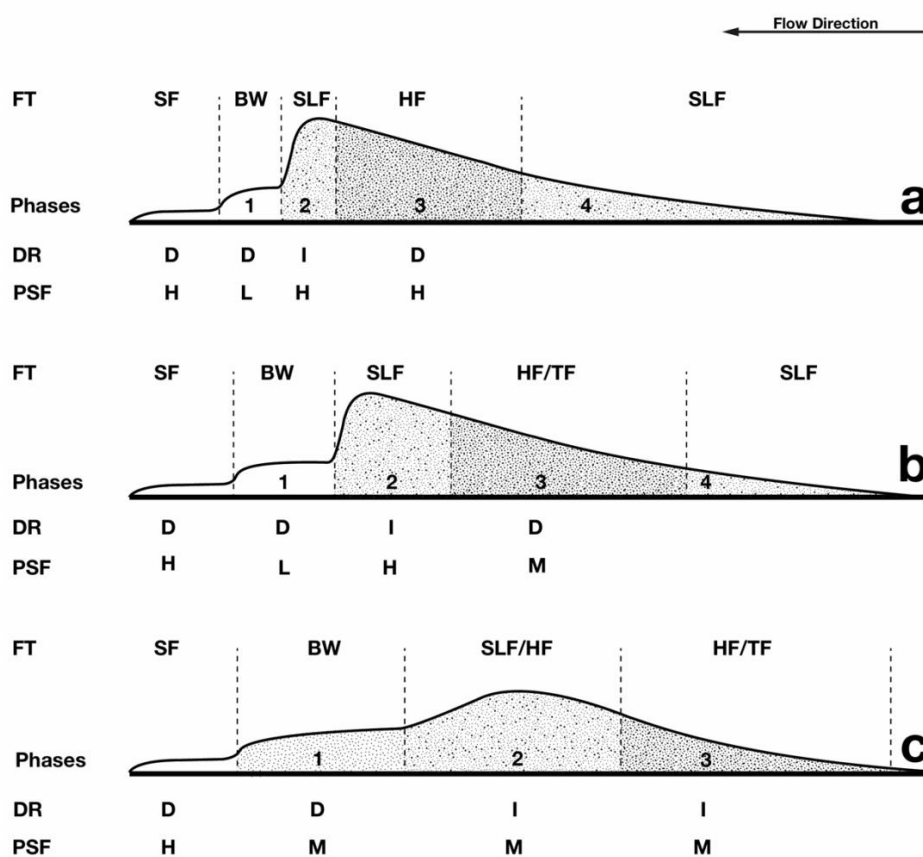


389 4.2 Implications for monitoring

390 The main goal of this research is to contribute in defining better monitoring criteria for
391 dangerous mass flow events. The data described above is part of a larger collection of
392 monitoring data collected over the entire length of the Whangaehu channel consisting of 21
393 monitoring sites and years of preparation (e.g. Manville and Cronin, 2007; Keys and Green,
394 2008). Due to this, the ability to accurately estimate the properties of the lahar at various
395 stages along its path is possible. When it comes to flow events of any size, the ability to
396 understand how the dynamics change with distance along the channel is important for warning
397 and future hazard mitigation. We show here that a lake-breakout event can start out as an
398 outburst flood, bulk up into a hyperconcentrated flow, then eventually elongate and entrap
399 enough sediment to transform into a plug-like slurry flow. Each of these flow types yields
400 differing PSF ranges and patterns due to the relationship between the channel geometry,
401 sediment concentration, turbulence, and bedload transport. While the lahar at different
402 stations along the channel may have differing PSF content, we also show that the lahar
403 elongates and a predictable model (e.g. Cronin et al., 1999) can be used with and shown in the
404 seismic data. Being able to apply such a model may yield some relevance of universality in
405 terms of warning systems at different distances away from source. Whereas shown above, the
406 flow phases at each monitoring stations can be seen, but at differing lengths and times in the
407 seismic signal (e.g. Figure 6). To better visualize this concept, conceptual models based off of
408 the Cronin et al., 1999 models are created for each of the three seismic stations for the 18
409 March 2007 lahar (Figure 8). In the conceptual models for the 2007 lahar, the aforementioned
410 elongation of the frontal pulse or bow wave (phase 1) and head of the lahar (phase 2) is shown,



411 along with the differences and similarities between the properties of the lahar at the three
 412 seismic monitoring sites.



413

414 *Figure 8 Conceptual models for the 18 March 2007 lahar at each of the three monitoring stations along the*
 415 *Whangaehu channel depicting flow type and the estimated seismic properties at each flow phase. a) RTMT 7.4 km*
 416 *from source, b) TRAN 28 km from source, and c) COLL 83 km from source. Flow types (FT) are as followed;*
 417 *streamflow (SF), bow wave streamflow (BW), hyperconcentrated flow (HF), Transitional flow (TF), and sediment-*
 418 *laden streamflow (SLF). Note, decreased (D), increased (I), high (H), low (L), and mixed (M) are notations for*
 419 *directionality ratios and peak spectral frequency estimates.*

420 Another implication for future warning is the implementation of 3-component sensors and the
 421 use of DRs for channels that have streamflow. Walsh et al. (2020) showed for lahars flowing in

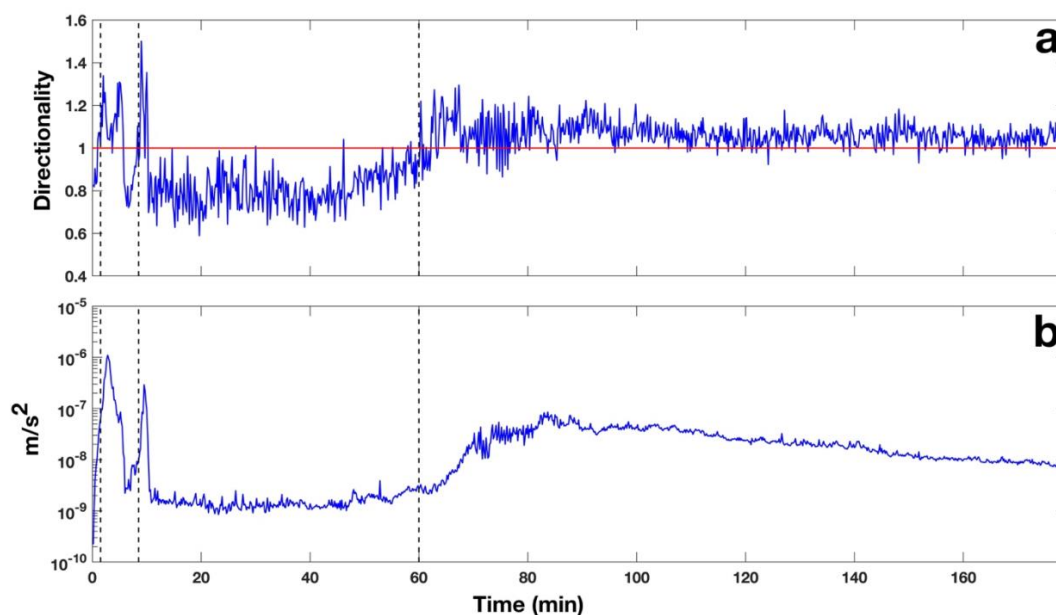


422 La Lumbre channel at Volcán de Colima that the DR for streamflow is <1 and then increases
423 when the lahar arrives. This same feature can be seen at each of the three monitoring sites for
424 the 18 March 2007 event (Figure 6) indicating differing flow types will still show this DR pattern
425 within the same flow and at other channels. To further show this, there were three natural non-
426 lake-breakout eruption-based lahars that occurred in the Whangaehu channel in September
427 2007 (for more details on the lahars see Cole et al., 2009; Kilgour et al., 2010) and recorded on
428 the seismometer at RTMT. The DR for the September events starts with streamflow with a DR $<$
429 1 and when the first lahar arrives the DR increases to >1 and as the lahar fully passes the DR
430 decreases to <1 again (Figure 9a). As the second lahar arrives at RTMT (Figure 9, second dashed
431 line), the DR increases to >1 again. After the second lahar passes the DR decreases once again
432 back below DR <1 . Finally, as the third lahar arrives (Figure 9, third dashed line) the DR yet again
433 increases above 1 for the entirety of the event.

434 For many mass flows and especially those that flow into channels with preexisting streamflow,
435 the peak seismic amplitude does not always coincide with the arrival of the mass flow, and thus
436 may not be the most reliable for event detection or warning. These observations may be due to
437 a frontal surge, the lag in sediment concentration or differences in peak amplitude with peak
438 discharge. Phase 1 (frontal streamflow surge) of the model proposed by Cronin et al. (1999) was
439 based on a hyperconcentrated flow interacting with streamflow, but has also been shown for
440 debris flows as well (e.g. Arratano and Moia, 1999). Arratano and Moia (1999) showed at
441 Moscardo Torrent, Italy, through a hydrograph that there was a precursory surge ahead of the
442 debris flow that was not seen in the seismic record. Similarly, at Ruapehu, for the 18 March
443 2007 lahar, at each of the three stations there is little evidence in the seismic amplitude that



444 there was a precursory surge or phase 1 (Figures 3-5, bottom panel). Conversely, the surge
445 ahead of the lahar can be seen in both the PSF analysis (drop to low frequencies) and in the DR
446 (decrease in DR) right before the peak seismic amplitude arrives. This shows that when
447 monitoring for future events that not only the amplitude should be used, but other analysis
448 (e.g. PSF, DR) as well, otherwise there could be a delay in the detection of an event.



449

450 *Figure 9 (a) Directionality ratio for the time sequence of the three lahars that occurred on 25 September 2007. (b)*
451 *RMS amplitude of the seismic record at RTMT during the timing of the three September lahars. Note that the black*
452 *dashed lines represent the timing of each lahar arriving at the monitoring site.*

453 Using all three components of the seismometer can be very beneficial in lahar monitoring. The
454 above-mentioned DR analysis can only be completed with horizontal recording, and analyzing
455 PSF in each component can yield critical information about the flow properties and dynamics.
456 Examining the seismic amplitude differences can generate significant discoveries, for example,
457 when the vertical component is stronger than the horizontal components, bedload dominates



458 over turbulence noise (Burtin et al., 2010). Greater flow parallel signals may indicate higher
459 water transport noises (Barrier et al., 2015) and higher cross-channel signals could be caused by
460 increased interflow particle collisions and flow-channel wall interactions (Doyle et al., 2010).
461 While using the differences in each component can be useful, there are also some concerns.
462 Channel geometry and bed conditions can alter the seismic signal (e.g. Coviello et al., 2019;
463 Marchetti et al., 2019). Additionally, the flow parallel direction can be influenced by the lahar
464 that has already passed, the lahar at the station and the lahar arriving. Furthermore, the tilt of
465 the seismometer may play a large role in determining which component is larger (e.g. Anthony
466 et al., 2018). In the case of the 18 March 2007 lahar a large pulse of water passed the stations
467 which may explain why the parallel component is stronger than the other two components at
468 RTMT and TRAN. At COLL, the lahar had elongated, lost energy, and thus shows more
469 decreased flow parallel energy compared to the previous two stations. In the cross-channel
470 direction, if a flow overtops the channel, the amplitude would presumably be dampened. This
471 may be the case at TRAN where both the flow parallel and vertical directions are more
472 energetic than the cross-channel amplitude after the passing of the head and breaking out of
473 the channel occurred (Figures 2d, 4 bottom row). Overall, these concerns can and should be
474 tested in the future to estimate potential error in these methods. Nevertheless, using all three
475 components of the seismometer can enhance the productivity of warning systems, and if
476 possible, should be used instead of single component sensors.

477 **5. Conclusions**



478 At 23:18 UTC on 18 March 2007 Mt. Ruapehu produced the biggest lahar in New Zealand in
479 over 100 years causing 1.3×10^6 m³ of water to flow out of the crater lake and rush down the
480 Whangaehu channel flowing for over 200 km to the Tasman sea. Seismic analysis at three
481 monitoring locations along the channel (7.4, 28, and 83 km) yielded an understanding of how
482 flow type and processes of the lahar evolve with distance. The proximal lahar was a highly
483 turbulent outburst flood, which generated high PSF content in all three components. Further
484 along the channel after the lahar had bulked up and transformed into a multi-phase
485 hyperconcentrated flow, the PSF content was variable and showed changes in the flow
486 regime/phase. Finally, at the most distal monitoring station, the lahar had lost energy and
487 transformed into a slurry-type flow where the PSF content became more bedload-dominant.
488 Additionally, directionality ratios from all three sites along with data from additional lahars
489 yielded strong evidence that DRs can be used for warning systems when there is streamflow
490 present in the channel. Furthermore, PSF and DRs show evidence of a pre-lahar water pulse
491 that is concealed in the raw seismic data, but has been observed visually. Ultimately, the use of
492 3-component broadband seismic analysis for the 18 March 2007 lahar at Mt. Ruapehu may lead
493 to more accurate and advanced real-time warning systems for mass flows through the use of
494 frequency and directionality around the world.

495 *Author Contribution*

496 BW performed seismic analysis and drafted the manuscript, CL organized and prepared data,
497 and JP created the visual location representation of the event. All participating authors



498 contributed to the discussions and editing of the draft of the manuscript, as well as approving
499 the final edition.

500 *Competing Interests*

501 The authors declare that they have no conflict of interest

502 *Acknowledgements*

503 This work was supported by the Resilience to Natures Challenges – New Zealand National
504 Science, volcano program of research. We would also like to thank all the people from Massey
505 University, Horizons Regional Council, NIWA, and the Department of Conservation that
506 collected data and set up monitoring locations all along the channel in preparation for and
507 during the lahar. A final special thanks to Kate Arentsen for editorial support.

508 **References**

509 Anthony, R., Aster, R., Ryan, S., Rathburn, S., Baker, M., 2018, Measuring mountain river
510 discharge using seismographs emplaced within the hyporheic zone, *Journal of Geophysical*
511 *Research: Earth Surface*, v. 123, p. 210-228.

512 Arattano, M., Marchi, L., 2005, Measurements of debris flow velocity trough cross-correlation
513 of instrumentation data, *Natural Hazards and Earth System Sciences*, v. 5, p. 137-142.

514 Arattano, M., Moia, F., 1999, Monitoring the propagation of debris flow along a torrent,
515 *Hydrological Sciences- Journal des Sciences Hydrologiques*, v. 44(5), p. 811-823.



- 516 Barriere, J., Oth, A., Hostache, R., Krein, A., 2015, Bed load transport monitoring using seismic
517 observations in a low-gradient rural gravel bed stream, *Geophys. Res. Lett.*, v. 42, p. 2294-2301.
- 518 Bartholomaus, T., Amundson, J., Walter, J., O'Neel, S., West, M., Larsen, C., 2015, Subglacial
519 discharge at tidewater glaciers revealed by seismic tremor, *Geophys. Res. Lett.*, v. 42, p. 6391-
520 6398.
- 521 Burtin, A., Vergne, J., Rivera, L., Dubernet, P., 2010, Location of river-induced seismic signal
522 from noise correlation functions, *Geophys. J. Int.*, v. 182, p. 1161-1173.
- 523 Capra, L., Borselli, L., Barley, N., Ruiz, J., Norini, G., Sarocchi, D., Caballero, L., Cortes, A., 2010,
524 Rainfall-triggered lahars at Volcan de Colima, Mexico: Surface hydro-repellency as initiation
525 process, *Journal of Volcanology and Geothermal Research*, v. 198, p. 105-117.
- 526 Capra, L., Coviello, V., Borselli, L., Marquez-Ramirez, V., Arambula-Mendoza, R., 2018,
527 Hydrological control of large hurricane-induced lahars: evidence from rainfall-runoff modeling,
528 seismic and video monitoring, *Nat. Hazards Earth Syst. Sci.*, v. 18, p. 781-794.
- 529 Carrivick, J., Manville, V., 2009, A fluid dynamics approach to modelling the 18th March 2007
530 lahar at Mt. Ruapehu, New Zealand, *Bull. Volcanol.* v. 71, p. 153-169.
- 531 Cole, S., Cronin, S., Sherburn, S., Manville, V., 2009, Seismic signals of snow-slurry lahars in
532 motion: 25 September 2007, Mt Ruapehu, New Zealand, *Geophys. Res. Lett.*, 36, L09405.
- 533 Coviello, V., Arattano, M., Comiti, F., Macconi, P., Marchi, L., 2019, Seismic characterization of
534 debris flows: Insights into energy radiation and implications for warning, *Journal of Geophysical*
535 *Research: Earth Surface*, v.124.



- 536 Coviello, V., Capra, L., Vazquez, R., Marquez-Ramirez, V., 2018, Seismic characterization of
537 hyperconcentrated flows in a volcanic environment, *Earth Surf. Process. Landforms.*, v. 43, p.
538 2219-2231.
- 539 Cronin, S., Neall, V., Jerome, L., Palmer, A., 1996, Unusual “snow slurry” lahars from Ruapehu
540 volcano, New Zealand, September 1995, *Geology*, v. 24, p. 1107-1110.
- 541 Cronin, S., Neall, V., Jerome, L., Palmer, A., 1999, Dynamic interactions between lahars and
542 stream flow: A case study from Ruapehu volcano, New Zealand, *GSA Bulletin*, v. 111, n. 1, p. 28-
543 38.
- 544 Cronin, S., Neall, V., Jerome, L., Palmer, A., 2000, Transformation, internal stratification, and
545 depositional processes within a channelized, multi-peaked lahar flow, *New Zealand Journal of*
546 *Geology and Geophysics*, v. 43, p. 117-128.
- 547 Doyle, E., Cronin, S., Cole, S., Thouret, J., 2010, The coalescence and organization of lahars at
548 Semeru volcano, Indonesia, *Bull. Volcanol.*, v. 72, p. 961-970.
- 549 Doyle, E., Cronin, S., Cole, S., Thouret, J., 2011, Defining conditions for bulking and debulking in
550 lahars, *GSA Bulletin*, v. 123, p. 1234-1246.
- 551 Huang, C., Shieh, C., Yin, H., 2004, Laboratory study of the underground sound generated by
552 debris flows, *Journal of Geophysical Research*, v. 109, F01008.
- 553 Iguchi, M., 2019, Proposal of estimation method for debris flow potential considering eruptive
554 activity, *Journal of Disaster Research*, v. 14(1), p. 126-134.



- 555 Gimbert, F., Tsai, V., Lamb, M., 2014, A physical model for seismic noise generation by turbulent
556 flow in rivers, *Journal of Geophysical Research: Earth Surface*, v. 119, p. 2209-2238.
- 557 Keys, H., Green, P., 2008, Ruapehu lahar New Zealand 18 March 2007: Lessons for hazard
558 assessment and risk mitigation 1995-2007, *Journal of Disaster Research*, v. 3, n. 4, p. 284-296.
- 559 Kilgour, G., Manville, V., Della Pasqua, F., Graettinger, A., Hodgson, K., Joly, G, 2010, The 25
560 September 2007 eruption of Mount Ruapehu, New Zealand: Directed ballistics, surtseyan jets,
561 and ice-slurry lahars, *Journal of Volcanology and Geothermal Research*, v. 191, p. 1-14.
- 562 Kogelnig, A., Surinach, E., Vilajosana, I., Hubl, J., Sovilla, B., Hiller, M., Dufour, F, 2011, On the
563 complementarity of infrasound and seismic sensors for monitoring snow avalanches, *Nat.*
564 *Hazards Earth Syst. Sci.*, v. 11, p. 2355-2370.
- 565 Kuehnert, J., Mangeney, A., Capdeville, Y., Vilotte, J., Stutzmann, E., Chaljub, E., et al., 2021,
566 Locating rockfalls using inter-station ratios of seismic energy at Dolomieu crater, Piton de la
567 Fournaise volcano, *Journal of Geophysical Research: Earth Surface*, 126, e2020JF005715.
- 568 Lube, G., Cronin, S., Manville, V., Procter, J., Cole, S., Freundt, A., 2012, *Geology*, v. 40, p. 475-
569 478.
- 570 Manville, V., Cronin, S., 2007, Breakout lahar from New Zealand's crater lake, *EOS Transactions*,
571 v. 88, n. 43, p. 441-456.
- 572 Manville, V., White, J., Hodgson, K., 2000, Dynamic interactions between lahars and stream
573 flow: A case study from Ruapehu volcano, New Zealand: Discussion and reply discussion, *GSA*
574 *Bulletin*, v. 112, n. 7, p. 1149-1152.



- 575 Marchetti, E., Walter, F., Barfucci, G., Genco, R., Wenner, M., Ripepe, M., McArdell, B., Price, C.,
576 2019, Infrasound array analysis of debris flow activity and implications for early warning,
577 *Journal of Geophysical Research: Earth Surface*, v. 124, p. 567-587.
- 578 Massey, C., Manville, V., Hancox, G., Keys, H., Lawrence, C., McSaveney, M., 2010, Out-burst
579 flood (lahar) triggered by retrogressive landsliding, 18 March 2007 at Mt Ruapehu, New Zealand
580 – a successful early warning, *Landslides*, v. 7, p. 303-315.
- 581 O'Connor, J., Clague, J., Walder, J., Manville, V., Beebee, R., 2020, Outburst Floods, *Reference*
582 *Module in Earth Systems and Environmental Sciences*, Elsevier.
- 583 O'Shea, B., 1954, Ruapehu and the Tangiwai disaster, *NZ J. Sci. Tech.* 36B, 174-189.
- 584 Pardo, N., Cronin, S., Palmer, A., Nemeth, K., 2012, Reconstructing the largest explosive
585 eruptions of Mt. Ruapehu, New Zealand: Lithostratigraphic tools to understand subplinian-
586 plinian eruptions at andesitic volcanoes, *Bull. Volcanol.*, v. 74, p. 617-640.
- 587 Pierson, T., Janda, R., Thouret, J., Borrero, C., 1990, Perturbation and melting of snow and ice by
588 the 13 November 1985 eruption of Nevado del Ruiz, Colombia, and consequent mobilization,
589 flow and deposition of lahars, *J. Volcanol. Geotherm. Res.*, v. 41(1), p. 17-66.
- 590 Pierson, T., Scott, K., 1985, Downstream dilution of a lahar: Transition from debris flow to
591 hyperconcentrated streamflow, *Water Resources Research*, v. 21, n. 10, p. 1511-1524.
- 592 Procter, J., Cronin, S., Fuller, I., Lube, G., Manville, V., 2010, Quantifying the geomorphic
593 impacts of a lake-breakout lahar, Mount Ruapehu, New Zealand, *Geology*, v. 38, p. 67-70.



- 594 Procter, J., Cronin, S., Sheridan, M., 2012, Evaluation of Titan2D modelling forecasts for the
595 2007 Crater Lake break-out lahar, Mt. Ruapehu, New Zealand, *Geomorphology*, v. 136, p. 95-
596 105.
- 597 Procter, J., Cronin, S., Fuller, I., Sheridan, M., Neall, V., Keys, H., 2010, Lahar hazard assessment
598 using Titan2D for an alluvial fan with rapidly changing geomorphology: Whangaehu River, Mt.
599 Ruapehu, *Geomorphology*, v. 116, p. 162-174.
- 600 Procter, J. N., Cronin, S. J., Zernack, A. V., Lube, G., Stewart, R. B., Nemeth, K., & Keys, H. (2014).
601 Debris flow evolution and the activation of an explosive hydrothermal system; Te Maari,
602 Tongariro, New Zealand. *Journal of Volcanology and Geothermal Research*, 286, 303-316.
- 603 Procter, J., Zernack, A., Mead, S., Morgan, M., & Cronin, S. (2021). A review of lahars; past
604 deposits, historic events and present-day simulations from Mt. Ruapehu and Mt. Taranaki, New
605 Zealand. *New Zealand Journal of Geology and Geophysics*, 64(2-3), 479-503.
- 606 Roth, D., Brodsky, E., Finnegan, N., Rickenmann, D., Turowski, J., Badoux, A., 2016, bed load
607 sediment transport inferred from seismic signals near a river, *J. Geophys. Res. Earth Surf. P.* 121,
608 725-747.
- 609 Schimmel, A., Coviello, V., Comiti, F., 2021, Debris-flow velocity and volume estimations based
610 on seismic data, *Natural Hazards and Earth System Sciences*.
- 611 Schmandt, B., Aster, R., Scherler, D., Tsai, V., Karlstrom, K, 2013, Multiple fluvial processes
612 detected by river side seismic and infrasound monitoring of a controlled floor in the Grand
613 Canyon, *Geophys. Res. Lett.* v. 40(18), p. 4858-4863.



- 614 Schmandt, B., Gaeuman, D., Stewart, R., Hansen, S., Tsai, V., Smith, J., 2017, Seismic array
615 constraints on reach-scale bedload transport, *Geology*, v. 45, p. 299-302.
- 616 Scott, K., 1988, Origins, behavior, and sedimentology of lahars and lahar runout flows in the
617 Toutle-Cowlitz river system, *USGS Professional Paper*.
- 618 Surinach, E., Vilajosana, I., Khazaradze, G., Biescas, B., Furdada, G., Vilaplana, J, 2005, Seismic
619 detection and characterization of landslides and other mass movements, *Natural Hazards and*
620 *Earth System Sciences*, v. 5, p. 791-798.
- 621 Walsh, B., Coviello, V., Capra, L., Procter, J., Marquez-Ramirez, V., 2020, Insights into the
622 internal dynamics of natural lahars from analysis of 3-component broadband seismic signals at
623 Volcán de Colima, Mexico, *Front. Earth Sci.* 8:542116.
- 624 Walsh, B., Jolly, A., Procter, J., 2016, Seismic analysis of the 13 October 2012 Te Maari, New
625 Zealand, lake breakout lahar: Insights into flow dynamics and the implications on mass flow
626 monitoring, *J. Volcanol. Geotherm. Res.*, v. 324, p. 144-155.